Aalborg Universitet

AALBORG UNIVERSITY

DENMARK

Comprehensive Investigation on Current Imbalance among Parallel Chips inside MW-Scale IGBT Power Modules

Wu, Rui; Smirnova, Liudmila; Wang, Huai; Iannuzzo, Francesco; Blaabjerg, Frede

Comprehensive Investigation on Current Imbalance among Parallel Chips inside MW-Scale IGBT Power Modules

Rui Wu*, *Student Member, IEEE,* Liudmila Smirnova†, *Student Member, IEEE,* Huai Wang*, *Member, IEEE,*
Francesco Iannuzzo*‡, *Senior Member, IEEE,* and Frede Blaabjerg*, *Fellow, IEEE*
*Center of Reliable Power Electronics (CORPE), Aalborg University, Denmark
†Department of Electrical Engineering, Lappeenranta University of Technology, Finland
‡DIEI, University of Cassino and southern Lazio, Italy
rwu@et.aau.dk, Lyudmila.Smirnova@lut.fi, hwa@et.aau.dk, fia@et.aau.dk, fbl@et.aau.dk.

Abstract—With the demands for increasing the power rating and improving reliability level of the high power IGBT modules, there are further needs of understanding how to achieve stable paralleling and identical current sharing between the chips. This paper investigates the stray parameters imbalance among parallel chips inside the 1.7 kV/1 kA high power IGBT modules at different frequencies by Ansys Q3D parastics extractor. The resulted current imbalance is further confirmed by experimental measurement.

Index Terms—Insulated-Gate Bipolar Transistor (IGBT), Power Modules, Current Imbalance, Finite Element Method.

I. Introduction

In modern power electronic systems, there is an increasing demand for improving the whole system endurance and safety level while reducing manufacturing and maintenance costs [1]. According to manufacturers' questionnaires [2], [3], semiconductor devices are considered the most critical and fragile component in industrial power electronic systems, the failure of which results in up to 34% of power electronic system failures. Because IGBTs are one of the most critical components as well as the most widely used semiconductor devices in industrial power electronic systems in the range above 1 kV and tens of kW [3], their reliability performance has drawn more and more attention.

At present, power modules are the most used packaging for IGBTs in modern medium and high power applications, for instance wind turbine systems [4]. Inside the IGBT power module, multiple chips are connected in parallel to increase the current rating. However, due to the chip characteristics as well as the layout design of the module [5], there could be a considerable current difference among the paralleled IGBT chips. This imbalance current sharing among the paralleled chips can be a reliability critical issue, because the consequent imbalance temperature will stress chips at different level and lead to lifetime mismatch among different chips. This challenge becomes even more critical for the MW-scale IGBT modules, due to the high current ratings (typically kA-level) and asymmetric geometry.

In the prior-art research, most focus is addressed on optimizing the current sharing among parallel connected IGBT power modules in order to construct reliable high current converters [6]–[10]. This can be achieved by designing bus bars with consideration of current coupling effects to minimize the stray parameters difference [6], [7], or by synchronizing IGBT switching signals to trigger IGBTs simultaneously [8], as well as adjusting the gate voltages and the gate resistances based on the thermal imbalance [9], [10]. However, these methods can be hardly applied in high power module construction, where a unique gate lead is connected to the several sections of the module [11]. An electromagnetic field analysis has been applied in [12] to investigate the current differences among 6 parallel IGBT chips based on a detailed structure description, while the mechanisms leading to this current difference have not been discussed. Partial Element Equivalent Circuit (PEEC) method has been applied to analyze the current imbalance of an IGBT module with 2 or 4 chips in parallel [13], [14], which shows that stray parameters extracted at specific frequency cannot reflect both the transient and on-state electrical behavior. The proposed lumped element equivalent resistance and inductance ladder can be used for predicting the electrical behavior inside the module [15], which needs fitting for hundreds of parameters, therefore it is quite time consuming. A recent study on medium power module shows that the module stray parameters difference can affect the power loss and temperature distribution among parallel IGBT chips [16]. Therefore, it is desirable to identify the stray parameters inside the MW level IGBT power module at different frequencies, and experimentally study the effects on the current distribution.

This study applies Finite Element Method (FEM) and Method of Moments (MoM) [17] in Q3D [18] to analyze the stray inductance and resistance of a 1.7 kV/1 kA IGBT power module at different frequencies. The setup and the corresponding measurement are also illustrated. This paper is organized as follows: Section II introduces the detailed structure and parameters of the studied IGBT power module. Section III describes the detailed principles of Q3D analysis,

the extracted stray parameters for different sections, as well as the corresponding PSpice simulating results. Section IV presents double pulse testing results of power modules from different manufacturers, which confirm the simulating results presented in Section III. The power loss distribution among the sections at different frequencies are also presented. Section V gives concluding remarks of the paper.

II. INFORMATION ABOUT THE STUDIED IGBT MODULE

This study focuses on a commercial 1.7 kV/1 kA IGBT module, which is widely used in wind turbine systems, motor drives and other high power converters. The main specifications are summarized in Table I.

The module package size is 234 mm by 89 mm by 38 mm. An outline picture is shown in Fig. 1(a). There are two power terminals for the DC plus connections (upper IGBT collector), two power terminals for the DC minus connection (lower IGBT emitter), one terminal with two screw connections for the output phase. The upper IGBT gate terminals are on the right side in Fig. 1(a), and the lower IGBT gate terminals are on the left side, which are also aligned with the thermal resistor connections. There are six sections connected in parallel to increase the current capability, and the definition of section numbers in this paper is shown in Fig. 1(b): the nearest section to the gate terminals is defined as section 1, while the farthest one is called section 6. Each section contains two IGBT chips and two freewheeling diode chips, which are configured as half-bridge for the standard applications.

The principle cross section of the power module is illustrated in Fig. 2. The package consists of a plastic frame and a metallic baseplate. The plastic frame is mechanically stable, and has high tensile strength within the whole temperature range. It is also electrically insulating, and ensures a long creepage distance at its surface. The silicone gel inside provides good electrical insulation properties. The module has a copper baseplate to provide fine thermal connection to the cooling medium. The Direct Copper Bonding (DCB) - substrate consists of a ceramic dielectric insulator with copper bonded to it. The DCB provides electrical insulation between the potential of the power devices and the potential of the heat sink, while providing good thermal connection to the heat sink. The upper copper layer of the DCB are also connected to copper bus bars. The metallic backside of the IGBT chip, the collector side, is soldered directly onto the upper copper layer. Bond wires on the top of the chip provide electrical connection to the gate and emitter contact of the chip. Aluminum (Al) bond wires are widely used, and the number of bond wires is determined by the rated current of the module.

In order to measure the current distribution, open power modules without the plastic frame and silicone gel are tested in this study. Each IGBT section is connected to the power terminals through copper bus bar, as shown in Fig. 2. The Rogowski coils can be easily inserted into the bus bars to measure each section's collector current.

Table I
MAXIMUM RATINGS AND SPECIFICATIONS OF THE IGBT MODULE UNDER INVESTIGATIONS.

| Specifications	Value
Collector-emitter voltage, V_{CES}	1700 V
Continuous DC collector current, I_{Cnom}	1000 A
Collector-emitter saturation voltage, V_{CEsat}	2 V
Total power dissipation	6.25 kW
Temperature under switching conditions	-40 °C $\sim$ 150 °C
Operation Temperature, T_{vjop}	150 °C
Rated short-circuit current, I_{SC}	4 kA
Gate-emitter maximum voltage, V_{GEs}	+/- 20V
Gate threshold voltage, V_{GEth}	5.8 V
Gate charge, Q_G	10 μC
Internal gate resistance, R_{Gint}	1.5 Ω
Number of parallel sections	6
Thermal resistance of junction to case, R_{thJC}	24 K/kW

(a)

(b)
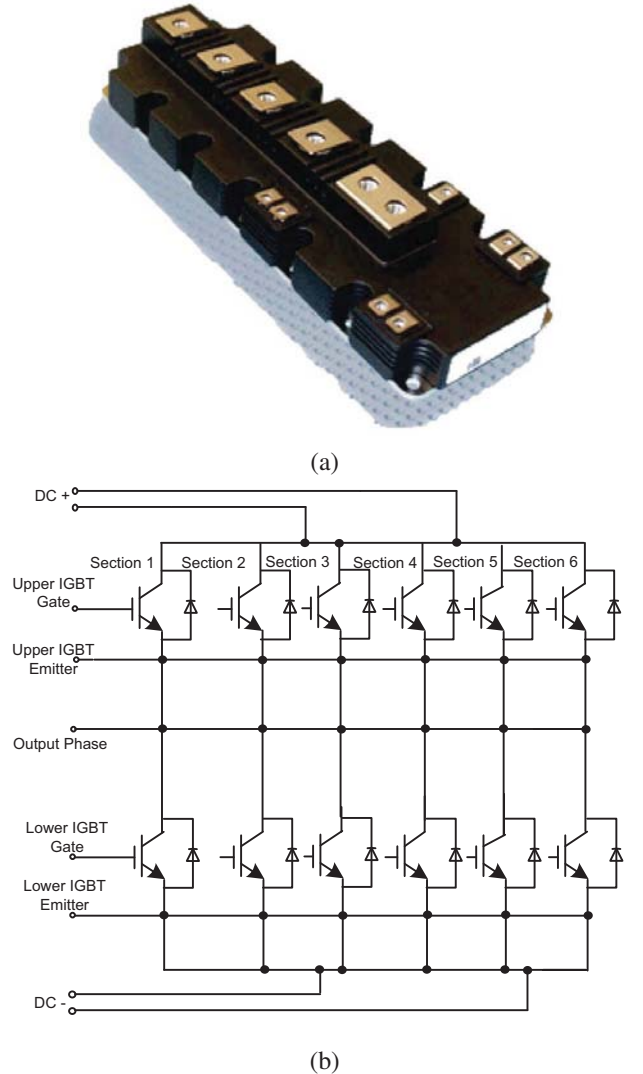
Figure 1. The studied IGBT power module (a) packaging outline picture, (b) internal structure of the power module with section definitions.
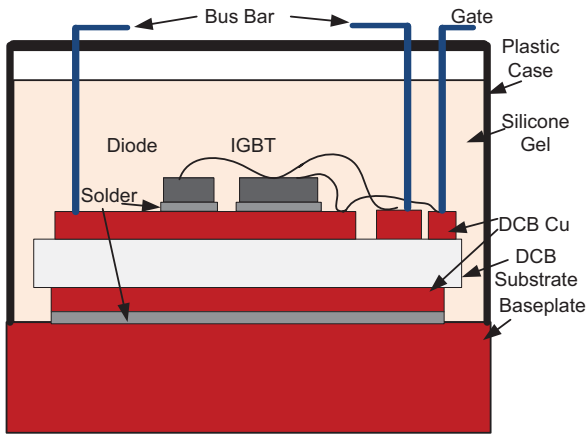
Figure 2. Cross section of the IGBT power module.

III. EXTRACTION OF STRAY PARAMETERS

At first, a detailed model should be constructed in FEM software, which should include the geometry and material information. A detailed geometry of the studied IGBT module is created in CAD program and then imported to the commercial software ANSYS/Q3D, which uses FEM and MoM to extract resistance, inductance and capacitance matrices. The structure built in Q3D is shown in Fig. 3, where the sources and sinks assigned are also indicated. The upper leg of the half-bridge module is studied in this paper (as shown in Fig. 1(b)). Simulations are performed in Q3D at different frequencies (1 kHz - 5 MHz), and the stray inductances (L_x) and resistances (R_x) of six sections (from the power terminals to each section) are extracted, as shown in Fig. 4. The simulations are done in such a way that, when extracting the inductance and resistance of a certain section, only the IGBT chip of this section conducts. For example, the current path is shown in Fig. 4 for the case when parameters of Section 1 are extracted and S_{11} (the section number is indicated by the second number of subscript) conducts. The simulation results at different frequencies are summarized in Table II.

It is worth noting that simulations should be performed at each frequency separately instead of the "frequency sweep" available in Q3D. This is because the finite element mesh for the adaptive solution is optimized for the simulated frequency only, so the accuracy of the results could vary at frequencies significantly far away from this solution frequency.

The difference in the inductances and resistances of different sections is observed. The results show that the middle section (section 2-4) have lower stray inductance and stray resistance than the other sections. It is noted that the stray inductance is almost constant with frequency, while the stray resistance increases with frequency rising due to skin and proximity effects. The imbalance of stray resistance is also higher at 5 MHz than 1 kHz. It means the current imbalance can be more obvious during switching transient, and particular sections may be more stressed and fail first under high frequency operations.

In order to study the imbalanced stray parameters effects on the electrical behavior, further PSpice simulations are
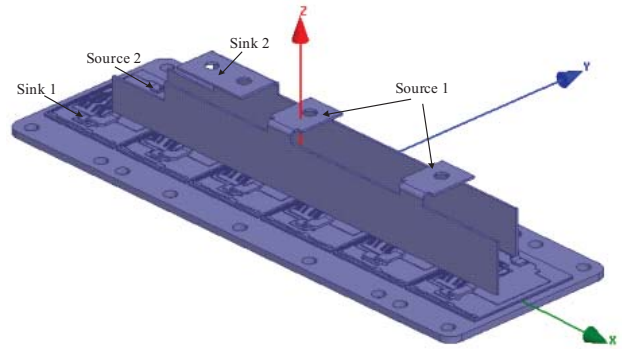

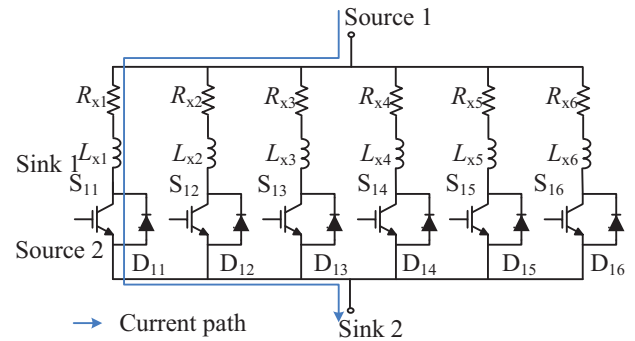Figure 3. The studied IGBT power module geometry in Q3D.

Figure 4. The circuit diagram of the upper leg of half-bridge IGBT module. The current path through the Section 1 is shown.

conducted based on the ANSYS/Q3D calculation results. Fig. 5 depicts the simulated circuit where the stray inductance and resistance of each section are included. The parameters of the components are estimated from the geometry of the physical module obtained by the aforementioned method. The adopted IGBT model is a lumped charge IGBT model, which demonstrated good accuracy [19]. The load inductance L_{Load} is 84 μH, and the freewheeling diode parameters are from the datasheet. Fig. 6 shows the turn-on waveforms under 600 V DC voltage. It is worth noting that the adopted parameters are the ones extracted under the specific IGBT switching frequency (i.e. 5 MHz), therefore the simulation results only accurately reflect the current sharing among parallel IGBTs during switching transient. For studying the current sharing during the conduction state, parameters at a lower frequency should be included in Fig. 5.

The PSpice simulation results are consistent with the Q3D analysis: sections 2-4 conduct more current than the other sections due to the lower stray inductance and resistance. Because sections 2-4 conduct higher current during transient, it can lead to more power loss. This imbalance phenomenon will be further investigated by the experiments in next section.

IV. EXPERIMENTAL VALIDATION

In order to validate the simulated results of the stray parameters' effects in the power module, experiments on current

Table II
THE STRAY RESISTANCE R_x AND INDUCTANCE L_x OF EACH SECTION'S POWER STAGE AT DIFFERENT FREQUENCY.

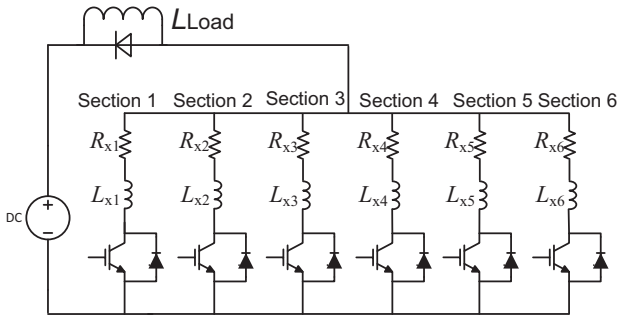| Frequency	Parameters	Section 1	Section 2	Section 3	Section 4	Section 5	Section 6
1 kHz	L_x (nH)	74	46	35	48	69	90
	R_x ($\mu\Omega$)	342	225	179	213	264	346
10 kHz	L_x (nH)	72	44	34	46	65	86
	R_x ($\mu\Omega$)	568	323	208	287	400	611
100 kHz	L_x (nH)	70	43	33	44	62	82
	R_x ($\mu\Omega$)	1449	850	469	665	931	1559
1 MHz	L_x (nH)	69	42	33	43	61	81
	R_x ($\mu\Omega$)	4301	2633	1524	1942	2711	4604
5 MHz	L_x (nH)	69	42	32	42	61	81
	R_x ($\mu\Omega$)	10065	6401	4645	5622	7457	10171

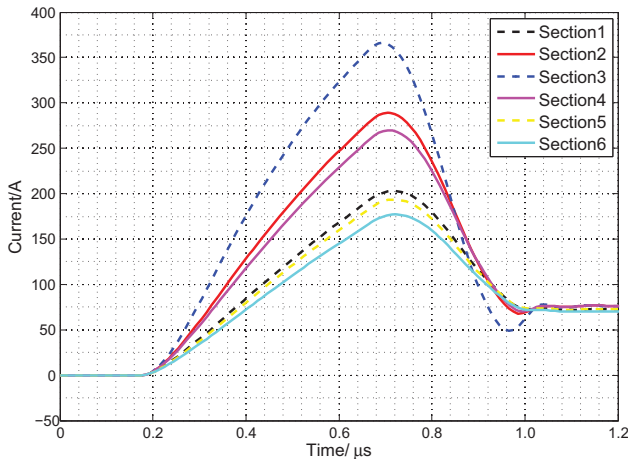Figure 5. The PSpice circuit for simulating the current imbalance during switching transient.

Figure 6. Simulated IGBT turn-on current among the 6 sections in the PSpice circuit of Fig. 5.

sharing inside the DUT have been conducted in the lab.

A. Testing Setup Description

Recently, several non-destructive testing concepts have been proposed to perform repetitive overcurrent and short circuit testing of IGBTs while avoiding significant device damage. A state-of-the-art non-destructive tester (NDT) with current and voltage limits of 6 kA and 1.1 kV has been constructed in the Device Characterization Laboratory of CORPE (Center of Reliable Power Electronics), Aalborg University [20].

A detailed electrical schematic of the NDT is shown in Fig. 7. Table III summarizes the specifications of the components. There are several components in parallel to enlarge the current capability and to minimize the stray inductance at the same time. In the same schematic, five Schottky diodes and an optional load inductance L_{Load} are present. The circuit is divided into two loops: Loop 1 is the main loop including the series protection, while Loop 2 includes the parallel protection. The Device under Test (DUT) is located in the common branch. The main difference with respect to traditional testing setup is the presence of an additional leg in parallel to the DUT, where a parallel protection is included together with a capacitor bank C_{NEG} and a negative battery V_{NEG}. The parallel protection has a twofold role: 1) to assist the series protection during its turn off by diverting the tail current of series protection IGBTs, and 2) to act as a crow-bar in case instability occurrence. To enhance its promptness and effectiveness, a negative bias is fed to its emitters by the battery V_{NEG} and the capacitors C_{NEG}. In this way, the typical large voltage tail at the turn on of the IGBT switches is accelerated and the voltage zeroes more promptly. To prevent supplying negative voltage to the DUT, Schottky diodes are placed in the circuit. The setup implementation in the lab is illustrated in Fig. 8. More details of the specifications and principle of the NDT can be found in [20].

The NDT can be also profitably used for an improved double pulse tests. In the double pulse tests, the series protection is deactivated and a 84 μH inductance L_{Load} is integrated. The first pulse is driven by parallel protection, and the second pulse is switched by the DUT. In this case, the self-heating effects on DUT due to the first pulse can be eliminated, so the DUT operates at a specific junction temperature.

The DUT is the 1.7 kV/1 kA IGBT module introduced in section II. The DUT is an open module without silicone gel, and a Rogowski coil is inserted into each IGBT section to measure single section currents. Modules from two manufacturers (module A and module B) with same ratings have been tested. A customised "Ultra mini CWT" Rogowski probe with custom coil length has been adopted for current measurements
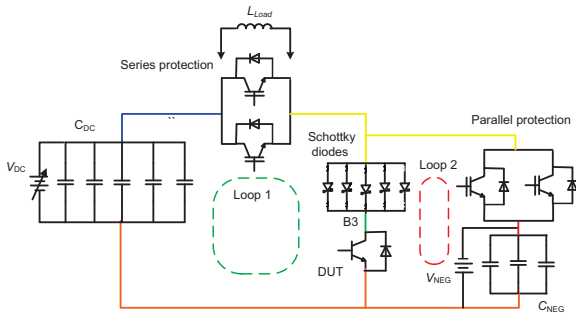
Figure 7. Detailed schematic of the Non-destructive Testing circuit.

Table III
RATINGS OF THE MAIN COMPONENTS IN THE CIRCUIT OF FIG. 7.

Characteristic	Value
DC Maximum voltage	1.1 kV
DUT Maximum current	6 kA
DC capacitors C_{DC}	5 x 1100 μF, 1100 V
Stray inductance of the main loop	37 nH
Series protection	2 x Dynex DIM1500ESM33-TS000 3 kA/ 3.3 kV
Parallel protection	2 x Mitsubishi CM1200HC-66H 2.4 kA/ 3.3 kV
Auxiliary capacitors C_{NEG}	3 x 1100 μF, 1100 V
Schottky diodes	5 x 170 V, 1.2 kA

owing to its non-intrusive behaviour (typical impedance in the range of a few pH) and its range of several kA [21].

B. Experimental Results

According to the simulation results in Section III, the stray parameters imbalance is identified among the parallel sections, which could lead to current imbalance during the switching
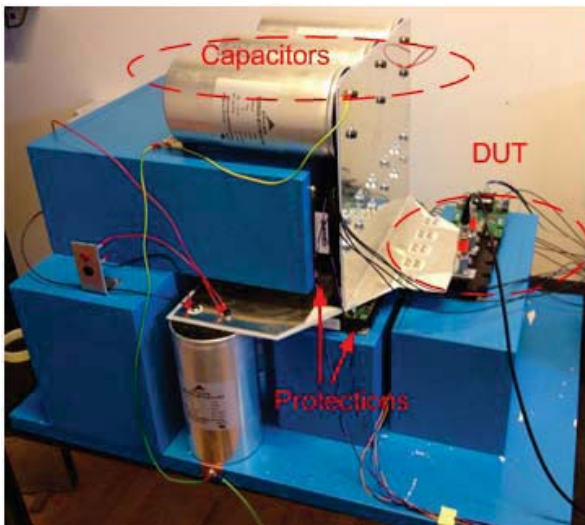

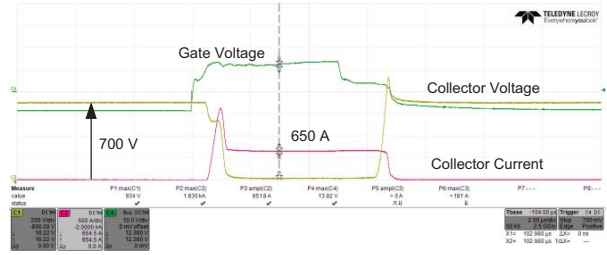Figure 8. The non-destructive testing setup in the lab.

Figure 9. Double pulse testing waveforms for module A at 700 V DC voltage. Time scale: 2 μs/div; Collector Voltage(C1): 200 V/div; Collector Current(C2): 500 A/div; Gate Voltage(C4): 10 V/div.
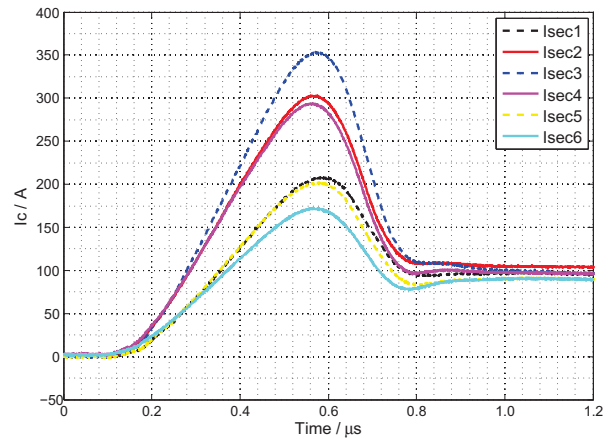

Figure 10. Measured current distribution among six sections of module A during turn-on transient.

transient. The freewheeling diode's reverse recovery current can lead to a current peak during the IGBT turn-on transient, which can be used for investigating the imbalance. In order to clearly evidence the current imbalance, the anti-parallel diode in the 3.3 kV IGBT series protection is adopted as freewheeling diode to achieve high current peak. Fig. 9 shows the experimental waveforms of the DUT from manufacturer A, where the collector voltage is 700 V.

In Fig. 10, the current distribution among the six sections of module A is illustrated at 600 V DC voltage, which has been measured by means of an equal number of Rogowski coils. A non perfect current balance among the six sections can be recognized especially during the turn-on transient. It is worth noting that the experimental current distributions are in good agreement with the PSpice simulation results in Fig. 6 based on the parameters from the Q3D analysis: sections 2-4 conduct more current than the other sections. Fig. 11 gives the calculation of different sections energy loss during the turn-on transient of Fig. 10. The turn-on loss of section 3 is almost twice of section 6. A further comparison of the accumulated energy loss with time is illustrated in Fig. 12. It can be seen that middle sections (2,3,4) have higher losses than the others. The obtained result could be very useful in many situations, e.g. to accurately design the cooling system in order to save design margin.
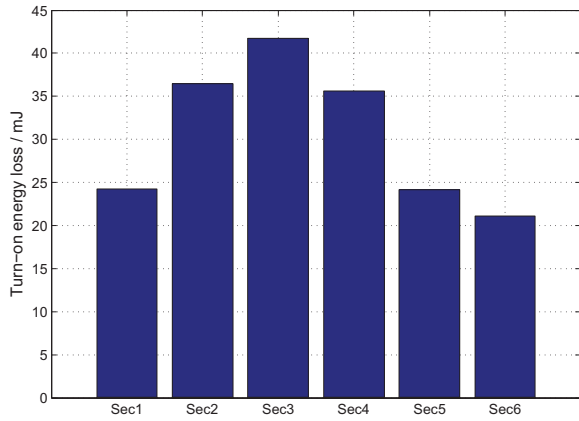
Figure 11. Measured turn-on energy loss distribution among the six sections obtained by Fig. 10.
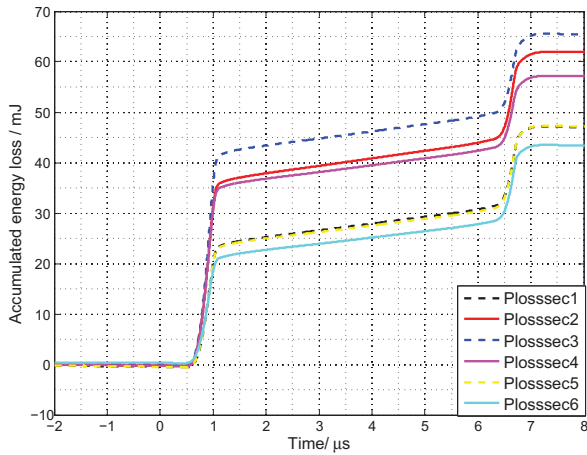

Figure 13. Total power loss (including switching loss and conduction loss) among six sections at different switching frequencies.

Figure 12. The measured accumulated energy loss among six sections along with time propagation (from time zero to the respective time instants).

Figure 14. Measured current distribution among six sections of module B at same condition of Fig. 10.

It is worth noting that the current during turn-on transient is more imbalanced than the current during on-state. This interesting results suggests that different loss distributions can be observed at different operating frequencies. In order to better investigate the frequency effects, a study case is proposed where the IGBT module is operated at different frequencies (i.e. 1 kHz, 5 kHz and 10 kHz) with a duty cycle of 50%. The total power loss (including switching loss and conduction loss) of the sections has been measured and reported in Fig. 13. At higher operating frequency, the total power loss increases significantly. It is worth pointing out that the experimental results are in good agreement with the predicted behavior: at increasing frequencies the imbalance slightly increases.

In order to check whether the observed current imbalance phenomenon is consistent among different technologies, another IGBT power module (module B) with the same ratings but from a different manufacturer has been tested at the same conditions. Even though module A and B have the same outline and connection, they have different internal structure
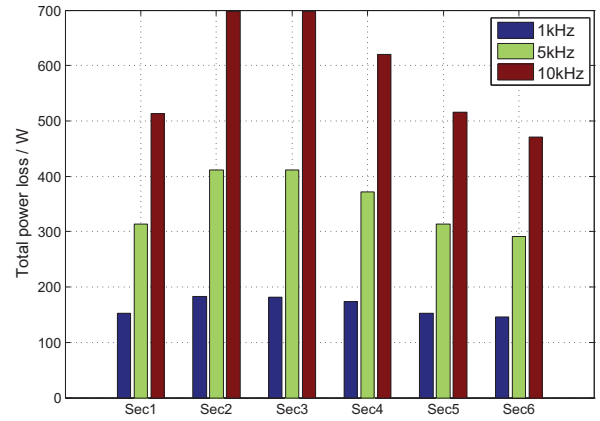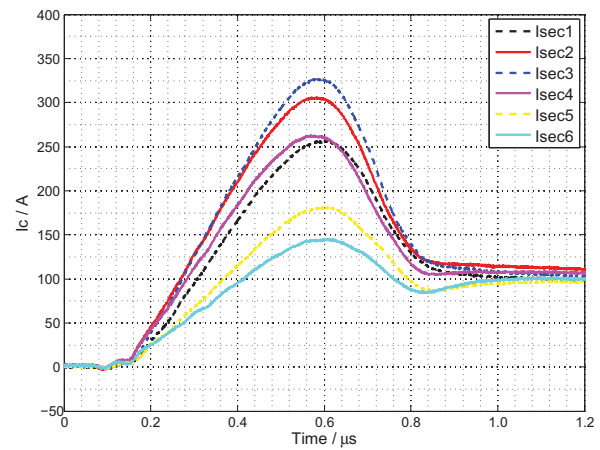
and geometry. Tests at same conditions are applied on module B, and the inside current distribution during turn-on is plotted in Fig. 14. Due to the internal design difference, the current distribution is slightly different from module A. By comparing Fig. 10 and Fig. 14, it can be seen that middle sections are slightly more stressed than the lateral ones. This similar current distributions reveal that there is some space for improving the current distributions inside such class of power modules. It also shows some improvement margins from the thermal management point of view.

V. CONCLUSION

This paper investigates the effects of the stray parameters imbalance among parallel chips inside the typical wind-turbine-scale IGBT power module by means of Q3D simulations. It has been shown that the stray parameters imbalance can lead to current imbalance among the parallel chips. Both simulations and experiments show that some chips are more stressed than others by the imbalanced power loss. Furthermore, the observed imbalance phenomenon is frequency-

dependent. The proposed study can provide a feedback to module designers on optimizing module's internal structure and geometry, as well as give suggestions for application engineers to improve the thermal management and/or cooling system design.

Acknowledgment

References

[1] H. Wang, M. Liserre, and F. Blaabjerg, "Toward reliable power electronics - challenges, design tools and opportunities," *IEEE Industrial Electronics Magazine*, vol. 7, no. 2, pp. 17–26, Jun. 2013.

[2] E. Wolfgang, "Examples for failures in power electronics systems," in *ECPE Tutorial on Reliability Power Electronic System*, 2007.

[3] S. Yang, A. T. Bryant, P. A. Mawby, D. Xiang, L. Ran, and P. Tavner, "An industry-based survey of reliability in power electronic converters," *IEEE Transactions on Industry Applications*, vol. 47, no. 3, pp. 1141–1451, May/Jun. 2011.

[4] F. Blaabjerg, M. Liserre, and K. Ma, "Power electronics converters for wind turbine systems," *IEEE Transactions on Industry Applications*, vol. 48, no. 2, pp. 708–719, May 2012.

[5] J. Lutz, U. Scheuermann, H. Schlangenotto, and R. D. Doncker, *Semiconductor power devices*, ser. ISBN: 3642111246. Springer, 2011.

[6] L. Popova, R. Juntunen, T. Musikka, M. Lohtander, P. Silventoinen, O. Pyrhonen, and J. Pyrhonen, "Stray inductance estimation with detailed model of the IGBT module," in *Proceedings of the 15th European Conference on Power Electronics and Applications (EPE)*, 2013, pp. 1–8.

[7] M. Paakkinen and D. Cottet, "Simulation of the non-idealities in current sharing in parallel igbt subsystem," in *Proceedings of Twenty-Third Annual IEEE Applied Power Electronics Conference and Exposition (APEC)*, 2008, pp. 211–215.

[8] N. Chen, F. Chimento, M. Nawaz, and L. Wang, "Dynamic Characterization of Parallel-Connected High-Power IGBT Modules," *IEEE Transactions on Industry Applications*, vol. 51, no. 1, pp. 539–546, Jan./Feb. 2015.

[9] J. Bohmer, J. Schumann, K. Fleisch, and H.-G. Eckel, "Current mismatch during switching due to the self-turn-off effect in paralleled IGBT," in *Proceedings of the 15th European Conference on Power Electronics and Applications (EPE)*, 2013, pp. 1–9.

[10] X. Wang, Z. Zhao, and L. Yuan, "Current sharing of IGBT modules in parallel with thermal imbalance," in *Proceedings of the 2010 Energy Conversion Congress and Exposition (ECCE)*, 2010, pp. 2101–2108.

[11] U. Schlapbach, "Dynamic paralleling problems in igbt module construction and application," in *Proceedings of 2010 6th International Conference on Integrated Power Electronics Systems (CIPS)*, 2010, pp. 1–7.

[12] K. Morishita, S. Kitamura, Y. Yamaguchi, H. Yamaguchi, Y. Nakayama, O. Usui, T. Ohi, and E. Thal, "Investigations of parallel connected IGBT's using electromagnetic field analysis," in *Proceedings of 2005 European Conference on Power Electronics and Applications*, 2005, pp. 1–5.

[13] K. Liang, Z. Jin, Q. Zhijie, and J. M., "Research and measurement of chip current imbalance in IGBT module with multiple chips in parallel," in *Proceedings of 2013 International Conference on Electrical Machines and Systems (ICEMS)*, 2013, pp. 1851–1856.

[14] J.-L. Schanen, C. Martin, D. Frey, and R.-J. Pasterczyk, "Impedance criterion for power modules comparison," *IEEE Transactions on Power Electronics*, vol. 21, no. 1, pp. 18–26, Jan. 2006.

[15] R. Azar, R. Udrea, T. N. Wai, F. Dawson, W. Findlay, and P. Waind, "The Current Sharing Optimization of Paralleled IGBTs in a Power Module Tile Using a PSpice Frequency Dependent Impedance Model," *IEEE Transactions on Power Electronics*, vol. 23, no. 1, pp. 206–217, 2008.

[16] Y. Zhong, J. Meng, P. Ning, D. Zhang, and X. Wen, "Comprehensive comparative analysis of two types of commonly-used layouts of IGBT packages," in *Proceedings of 17th International Conference on Electrical Machines and Systems (ICEMS)*, 2014, pp. 1952–1956.

[17] S. Rao, D. Wilton, and A. Glisson, "Electromagnetic scattering by surfaces of arbitrary shape," *IEEE Transactions on Antennas and Propagation*, vol. 30, no. 3, pp. 409–418, May 1982.

[18] ANSYS®, "Q3d extractor, v 6.0, user guide," ansys, inc., Tech. Rep.

[19] F. Iannuzzo and G. Busatto, "Physical cad model for high-voltage igbts based on lumped-charge approach," *IEEE Transactions on Power Electronics*, vol. 19, no. 4, pp. 885–893, Jul. 2004.

[20] R. Wu, L. Smirnova, F. Iannuzzo, H. Wang, and F. Blaabjerg, "Investigation on the short-circuit behavior of an aged IGBT module through a 6 kA/1.1 kV non-destructive testing equipment," in *Proceedings of 40th Annual Conference of the IEEE Industrial Electronics Society (IECON)*, 2014, pp. 3367–3373.

[21] W. Ray and C. Hewson, "High performance Rogowski current transducers," in *Proceedings of IEEE Industry Applications Conference*, vol. 5, 2000, pp. 3083–3090.